scientific reports

Check for updates

OPEN

Enhancing the pull-out behavior of ribbed steel bars in CNT-modified UHPFRC using recycled steel fibers from waste tires: a multiscale finite element study

Majid Pouraminian[1], Amir Ebrahim Akbari Baghal[2], Keyvan Andalibi[3], Farshid Khosravi[4]✉ & Vahid Arab Maleki[5]✉

In the current investigation, the effect of recycled steel fibers recovered from waste tires on the pull-out response of ribbed steel bars from carbon nanotube (CNT)-modified ultrahigh performance fiber reinforced concrete (UHPFRC) was considered using the multiscale finite element method (MSFEM). The MSFEM is based on three phases to simulate CNT-modified UHPC, recycled steel fibers (RSFs), and ribbed steel bars. For the first time, a bar ribbed has been simulated to make more realistic assumptions, and RSFs have been distributed in the form of curved cylinders of different lengths and with a random distribution within a concrete matrix. The interaction of the steel bar and the RSFs with the concrete is applied by the cohesive zone model (CZM). After confirming the simulation outcomes with the experimental results, the steel bar pull-out response is investigated using load-slip curves. The impact of the CNT content, RSFs and their aspect ratio on the bond strength of steel bars and CNT-modified UHPFRC was assessed. The results show that using RSFs with a lower aspect ratio (steel microfibers) significantly improves the pull-out characteristics of steel bars from concrete. Accordingly, the proposed MSFEM is considered for simulating the effects of different parameters on the pull-out response of ribbed steel bars from concrete without causing complex, time-consuming, or costly experiments. The results indicated that waste fiber or RSF can be used as a toughening component in CNT-modified ultrahigh-performance concrete and as a replacement for industrial steel fibers.

Keywords Carbon nanotube, Irregular steel fiber, Ultrahigh-performance fiber reinforcement concrete, Finite element method, Bond behavior

Fiber-reinforced concrete is generally used to increase the dynamic behavior of concrete structures exposed to earthquakes, blasts, and impacts in military, passive defense, and retrofit projects[1–3]. In addition to improving the toughness and ductility of concrete, fibers also improve its flexural and tensile strength, as well as its resistance to impact and dynamic loads. This reduces concrete fragmentation and crack propagation[4]. As the use of this kind of concrete has developed recently, the analysis of its performance from various perspectives has received much attention[5–7].

Since fiber-reinforced concrete is a composite material, its mechanical properties depend on the characteristics of the fibers (volume fraction, stiffness, geometrical properties, aspect ratio, and parameters of fiber bonding), concrete characteristics (compressive strength and type of materials), and other concrete additives, such as nanoparticles or pozzolanic materials[8]. Nguyen et al.[9] investigated the different curing conditions and mixed design factors of UHPC and their effects on the elastic modulus and strength of UHPC. Using different curing conditions, they reached a compressive strength of 200 MPa for UHPFRC. Banthia et al.[10] studied the impact

[1]Department of Civil Engineering, Ramsar Branch, Islamic Azad University, Ramsar, Iran. [2]Department of Civil Engineering, Bostan Abad Branch, Islamic Azad University, Bostan Abad, Iran. [3]Department of Civil Engineering, University of Tabriz, Tabriz, Iran. [4]Mechanical Engineering Department, Faculty of Engineering, Manisa Celal Bayar University, Manisa, Turkey. [5]Department of Mechanical Engineering, University of Maragheh, Maragheh, Iran. ✉email: Farshid.khosravi09@gmail.com; Vahid_maleki@tabrizu.ac.ir

of micro cellulose and steel fibers on the compressive strength of concrete. In this study, fibers were used alone and in combination in the specimens. In specimens where cellulose fibers are used alone, the fibers lose their efficiency due to the small length of large cracks. Therefore, concrete specimens have low flexural strength and energy absorption. According to this study, cellulose fibers alone do not increase the mechanical properties of the specimens, but in specimens that use hybrid steel and cellulose fibers, the flexural strength and toughness increase. Sabbaghian and Kheyroddin[11] studied the impact of fibers and age on the mechanical characteristics of fiber-reinforced cementitious materials. The results show that adhesion among fibers and the matrix at the joint surface, in general, can be frictional or chemical and frictional-chemical. Fiber bonding depends more on the fiber material, which depends on the fiber surface modification methods and matrix properties. The effect of using recycled and industrial steel fibers on concrete reinforcement was investigated experimentally by Ghone et al.[12]. Isa et al.[13] researched the impact of RSF usage on the mechanical characteristics of UHPC. In their study, mechanical properties were obtained for 2%, 3%, and 4% by volume fraction of fibers. Based on their research, RSFs provide improved mechanical properties and are environmentally friendly. Pertan et al.[14] studied the impact of adding polypropylene and forta fibers on the compressive strength, Young's modulus, crack pattern, and absorbed energy of cylindrical samples. They used the digital image correlation (DIC) method to investigate the displacement and deformation of the specimens more accurately and used Abaqus finite element software to validate these results. In finite element modeling, fiber-reinforced concrete is considered an isotropic material. Huang et al.[15] investigated the impact of carbon nanotubes and graphene nanosheets on the mechanical characteristics of UHPC. Their study showed that carbon nanotubes have a more favorable impact than graphene nanosheets. Although UHPFRC has good mechanical properties, in some cases, it is necessary to use steel bars for rising the load-bearing capacity of this type of concrete. These studies indicate that the mechanical characteristics of UHPC vary depending on the bonding behavior of steel ribbed bars to the concrete matrix, the geometric shape of the steel ribbed bar and the compressive strength. Zhao and Xiao[16] studied the bonding behavior of coated steel bars and UHPFRC concrete and presented an analytical model to estimate the load−displacement curves. The bonding behavior between steel bars and ordinary concrete and UHPFRC was studied by Khaksefidi et al.[17]. Using the pull-out test, they extracted the load–displacement curves for different specimens and studied the influence of some parameters on the pull-out load. Since performing experimental tests in this field has time constraints and high costs, in recent years, the use of FEM to predict the mechanical behavior of materials has developed[18,19]. They used the three-dimensional nonlinear MSFEM to perform simulations and simulated the relationships among fibers and the matrix via the cohesive zone model (CZM). Their study showed that bonding between fibers and the concrete matrix is affected by various parameters, including the direction and length of the fibers, the geometric shape of the fibers, and the strength of the concrete matrix. Accordingly, in numerical modeling, for concrete and fibers to work together properly, a law must be created that accurately reflects the characteristics of this interfacial transition zone (ITZ). Karimzadeh et al.[20] suggested a computational model to predict the mechanical achievement of nanotube/polymer composites. Continuum and finite element mechanics are used to model the interaction between the nanotube and the matrix. Multiscale modeling was suggested by Ayatollahi et al.[21] to predict the nonlinear characteristics of polymer nanocomposites under tensile, flexural, and torsional loads. In their proposed model, the intermediate phase is continuously simulated, and different Young's moduli are assumed. Their study revealed that the mechanical characteristics of the interface between the fibers and the matrix have little impact on the stiffness of the nanocomposite. Nevertheless, the fiber aspect ratio has a large influence on the Young's modulus. Esmaeili et al.[22] studied the release of steel fibers from polymer composites using different multiscale FEMs and considered the various components used in concrete, considering various geometric shapes of the fiber ends. Their study proposed a new algorithm for the random dispersal of fibers within polymer bodies. Bouhala et al.[23] determined the failure parameters of composites using the CZM-based inversion method and the FEM. In this method, the thickness of the interfacial elements was assumed to be zero, and by defining the fracture properties, the separation behavior of the fibers and the matrix can be simulated. Due to the accuracy of this method, in the present paper, the interface between the matrix and fibers with the CZM will be simulated.

To date, the pull-out performance of steel bars from UHPC containing RSFs modified with carbon nanotubes has not been studied. Accordingly, for the first time, in the present work, the impacts of different parameters of RSF waste tires on the bond strength of ribbed steel bars and carbon nanotube-modified UHPC were investigated. This study uses the multiscale finite element technique and an experimental pull-out test. For this purpose, first, the tensile strength, elastic modulus, and compressive strength of UHPC containing different volume fractions of carbon nanotubes are determined experimentally. Then, the steel bar pull-out test is applied. A multiscale finite element model was developed by considering the mechanical characteristics of UHPC modified with carbon nanotubes. ABAQUS finite element software is used to simulate reinforced concrete reinforced by RSFs. To simulate the chemical bonding of ribbed steel bars and RSFs with carbon nanotube-modified UHPC, the CZM is used, and the factors of this behavioral model are regulated using pull-out test results. Finally, the impacts of several factors, such as the fiber volume fraction, ribbed steel bar diameter, and amount of carbon nanotubes, on the bond characteristics of steel bars with UHPFRC are discussed. An evaluation of the proposed MSFEM was performed by comparing the predicted and experimental results, and the accuracy of the model was evaluated.

Experimental program

In this section, the process for producing carbon nanotube-modified UHPC and the experimental tests conducted for ribbed steel bar pull-out are described. The production of carbon nanotube-modified UHPC involves several steps. Initially, UHPC is prepared by mixing cement, fine aggregates, water, and additives according to the desired mix proportions. Then, carbon nanotubes (CNTs) are dispersed uniformly within the UHPC matrix

using suitable dispersion techniques such as sonication or mechanical mixing. The CNTs enhances the mechanical properties and durability of UHPC, making it suitable for various structural applications.

After the production of CNT-modified UHPC, experimental tests for ribbed steel bar pull-out were applied to evaluate the bond strength between the steel reinforcement and the concrete matrix. In these tests, ribbed steel bars are embedded within the CNT-modified UHPC specimens, and a pull-out load is applied to the steel bars until failure occurs. The pull-out force is measured and used to calculate the bond strength between the steel bar and the concrete matrix. These experimental tests provide valuable insights into the bond strength performance of CNT-modified UHPC, which is crucial for assessing its suitability for structural applications such as reinforced concrete elements in buildings and bridges. Additionally, the results of these tests can guide the optimization of CNT dispersion techniques and mix proportions to further enhance the mechanical characteristics and durability of UHPC.

RSF properties

Figure 1 illustrates the steel fibers recovered from waste tires utilized as reinforcement in concrete. The RSFs are made of St37 steel, and the mechanical and geometric characteristics of the fibers are presented in Table 1. Since RSFs have different lengths, to obtain the fiber length distribution, the image processing method used with optical methods and digital image correlation for a set of recycled fibers with 1500 pieces and experimental specimens of fiber distribution recycling and statistical analysis is given in Fig. 1 and Table 2.

Mix design

In the multiscale finite element model, CNT-modified UHPFRC is considered a separate and homogeneous phase. The mechanical properties used in the finite element analyses are extracted via experimental testing. Three cubic specimens with dimensions of $15 \times 15 \times 15$ cm^3 were made to test the compressive strength of each mixture. After molding, the specimens were constricted on a vibrating table and kept for 24 h in the curing cabin. Then, they were removed from the molds and kept under curing conditions until the age of the experiment. Finally, uniaxial compressive strength tests were applied on the specimens whose 28-day compressive strength was approximately 150 MPa. Figure 2 presents an SEM image of carbon nanotubes and the distribution of carbon nanotubes in the UHPC body. The final mixing design is selected according to the compressive strength, and

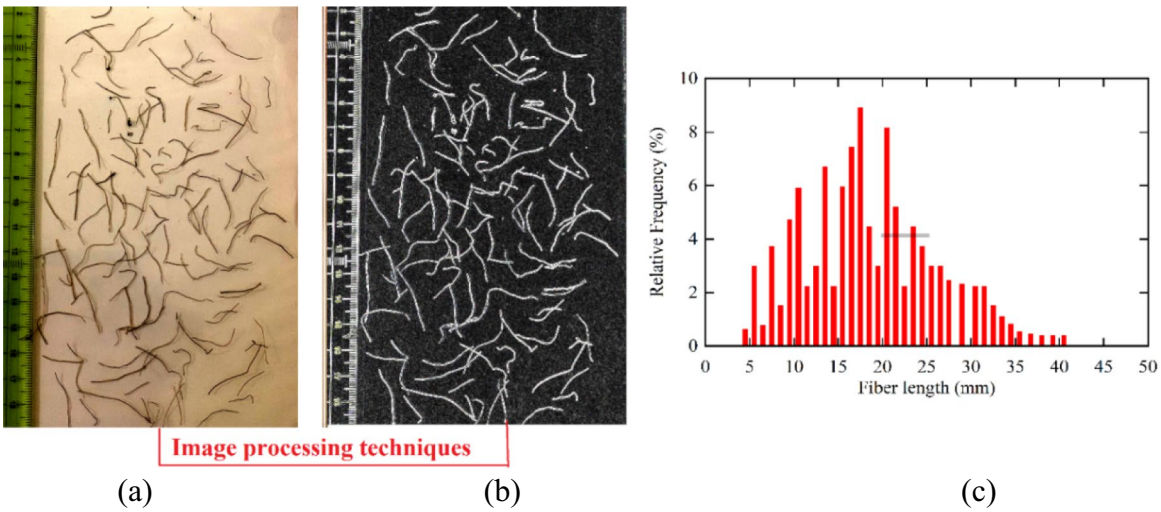

Figure 1. (**a**) Geometry of the recycled steel fibers, (**b**) image processing steps for the detected lines of the RSFs, and (**c**) length distribution.

Fiber type	d	f_t	f_p	E
Recycled steel-fiber	0.22 mm	240 MPa	430 MPa	200 GPa

Table 1. Geometrical and mechanical characteristics of the RSF.

	Fiber length							
Property	< 14 mm	14–30 mm	> 30 mm	Mean	Skewness	Kurtosis	Variance	SD
Value	34.13%	60.20%	5.67%	17.5	0.3857	2.8	0.4678	0.6835

Table 2. Statistical analysis of the RSF distribution.

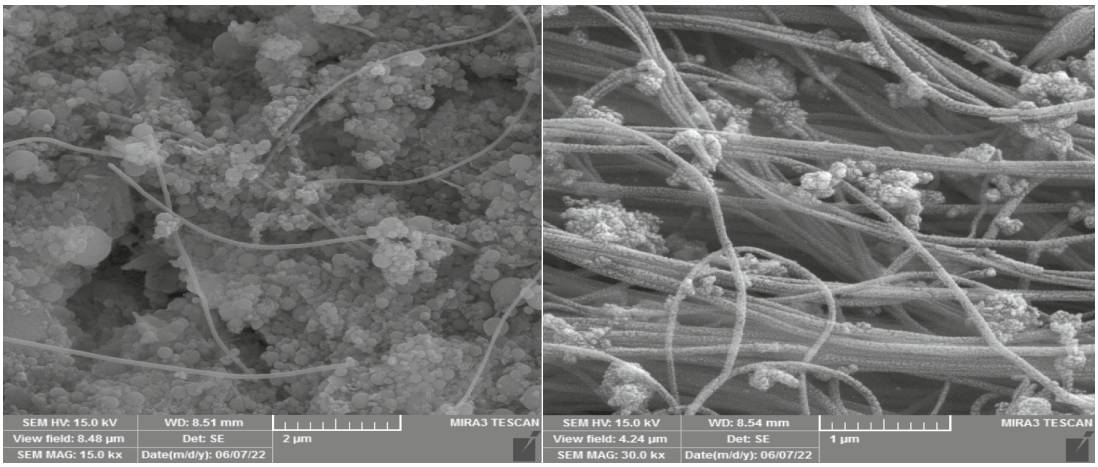

(a) **(b)**

Figure 2. (**a**) SEM image of carbon nanotubes and (**b**) SEM image of the dispersion of carbon nanotubes in the UHPC mixture/sample.

its specifications are listed in Table 3. To increase the mechanical characteristics of UHPC, carbon nanotubes with three different weight fractions of cement, 0.2, 0.4, and 0.8 wt.%, were used in the experiments. Carbon nanotubes were added to the water and dispersed using an ultrasonic device. Then, CNT-modified water was added to the UHPC mixture during the mechanical mixing stage. SEM images of CNTs and UHPFRC modified with CNTs are shown in Fig. 2.

Ribbed steel bar

In this study, steel bar pullout was tested with ribbed steel bars 14 mm in diameter according to ASTM A615 with a yield strength of 440 MPa. The stress−strain curve of the steel bar was calculated via tensile testing in accordance with the ASTM A615 standard and is presented in Fig. 3.

Steel bar pull-out test

According to RILEM-RC6[24,25], the concrete specimens used in the present study had dimensions of $150 \times 150 \times 150$ mm, and the geometric features of the specimens are presented in Fig. 4. According to Fig. 4, in this configuration, the concrete specimens are placed on a steel box, and the steel bar free end is fixed inside the machine's jaws. The experiment was performed on a universal testing device with a rate of 0.2 mm/min and a maximum load capacity of 1000 kN. As shown in Fig. 4, an LVDT displacement sensor was used to measure the displacement of the steel bar relative to the UHPC specimen by placing the sensor on top of the concrete specimen. The measured displacements indicate the slip among the steel bar and specimen. Finally, by performing an experimental test, the force-slip curve for a UHPC specimen with 1% recycled steel fibers and 0.2 wt. % CNTs was obtained.

Multiscale finite element simulations

In this study, the numerical simulation was conducted using a meso-scale finite element method (MFEM). This approach involves three distinct phases to simulate the CNT-modified ultra-high-performance concrete (UHPC), recycled steel fibers (RSFs), and ribbed steel bars. The MFEM captures the detailed interactions and mechanical behavior within each phase without explicitly addressing the correlation between different scales. This method enables a detailed analysis of local interactions, providing valuable insights into the mechanical performance of the composite material. Specifically, the CNTs were modeled to interact with the UHPC matrix, the RSFs were

(kg/m^3)	Mix design properties
700	Cement (type II)
300	Quartz powder
180	Micro-SiO_2
175	Water
1000	Silica sand
20	Super-plasticizer
0, 0.7	RSFs

Table 3. Mix design.

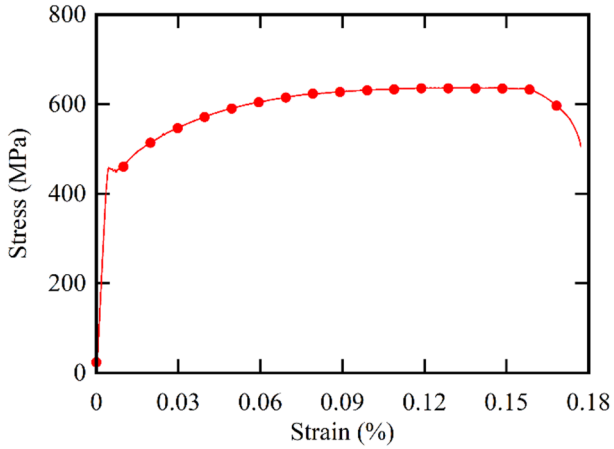

Figure 3. Steel rebar stress–strain curve based on the ASTM A615 standard test.

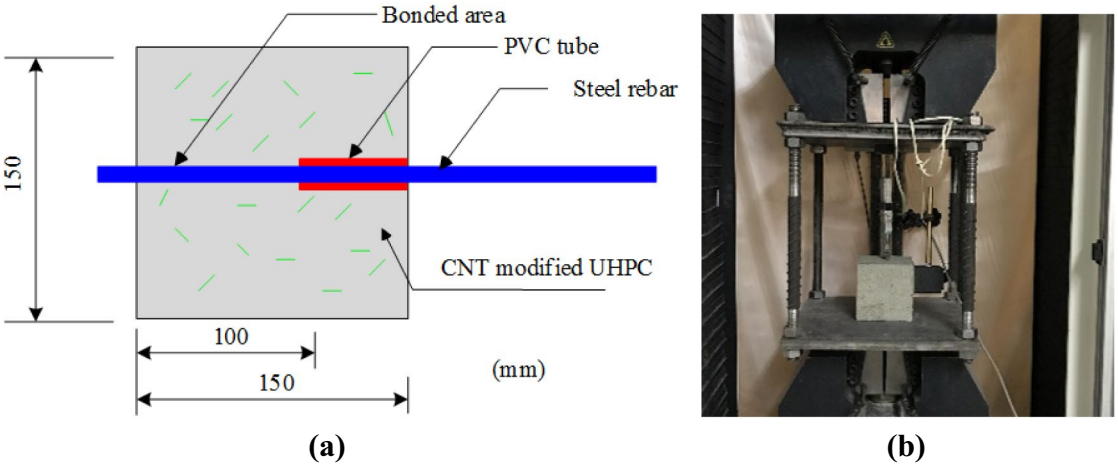

Figure 4. (**a**) Pull-out test details and (**b**) test setup device.

distributed randomly within the concrete matrix, and the ribbed steel bars were simulated to include mechanical interlocking effects.

The main aim of this investigation is to develop an MSFEM to determine the pull-out performance of ribbed steel bars from UHPC reinforced with waste tire steel fibers. In the multiscale simulation, the UHPFRC comprises three different parts: RSFs, CNT-modified UHPC, and the joint surface of fibers and concrete. RSFs are simulated as curved cylinders with different lengths and constant diameters. Due to the variability of the length of this type of fiber, in the simulation, similar to the results of image processing performed on fibers, the length of the samples is produced according to the statistical distribution shown in Fig. 1. Additionally, CNT-modified UHPC is considered a rectangular cube with homogeneous and uniform materials, and its mechanical properties have been determined for three different amounts of carbon nanotubes from experimental testing on laboratory specimens. To produce the geometric model of the fiber composite, the fibers are randomly distributed in the model, and then the volume of the set of fibers is removed from the concrete cube. The details of the finite element simulation are given below.

Generate fibers by random distribution

In our study, the random distribution of RSFs within the concrete matrix is a critical aspect of the MSFEM approach. To simulate this distribution accurately, it is essential to consider probabilistic models that can account for the inherent randomness in fiber orientation and placement. For this purpose, we refer to the work of Xiao et al.[26], which discusses probabilistic models applied to concrete corrosion depth prediction under sulfuric acid environments. This reference provides a relevant framework for incorporating probabilistic methods using 3D laser scanning technology.

In our study, RSFs of varying geometric shapes were incorporated into the concrete matrix to enhance its mechanical properties. The fibers used in our simulations were modeled as curved cylinders with different lengths and aspect ratios, which were randomly distributed within the UHPC matrix. The spatial curves of the fibers were generated using a probabilistic approach to ensure a realistic random distribution. For more realistic modeling,

the length of recycled fibers, which varies in practice, is determined using image processing techniques to obtain a statistical distribution. The following steps were employed to generate the random fibers:

Geometric modeling
According to the actual shape of the fibers, Each RSF was modeled as a curved cylindrical segment. The curvature and length of the fibers were varied to reflect the actual variability observed in recycled fibers. The curvature was defined using a random sinusoidal function to simulate the natural curvature of the fibers. Since RSFs have variable lengths and are shaped like curved cylinders, an accurate numerical model was created to simulate them as wires with a circular cross-section of a constant diameter (0.2 mm) and varying lengths, following the statistical length distribution shown in Tables 1, 2 and Fig. 1c. Initially, a specific number of fibers was considered based on the desired volume fraction of fibers. The lengths of these fibers were then assigned according to the distribution in Fig. 1c, and the volume fraction of the resulting fiber batch was calculated. If the volume fraction was less than required, additional fibers were added, and this process was repeated until the desired volume fraction was achieved.

Random distribution
To achieve a random spatial distribution, a probabilistic algorithm was implemented. This algorithm randomly positioned the fibers within the concrete matrix, ensuring that the orientation and placement of each fiber varied. The random distribution was generated using a uniform probability density function, which ensured that the fibers were uniformly dispersed throughout the matrix.

Overlap avoidance
To prevent unrealistic overlapping of fibers, a minimum distance constraint was applied between adjacent fibers. This constraint ensured that the fibers were randomly distributed while maintaining a realistic spatial arrangement.

Implementation in FEM
The randomly generated fiber geometries were then incorporated into the finite element model. The interaction between the fibers and the UHPC matrix was modeled using cohesive zone elements to simulate the bond behavior accurately.

This fiber design process was performed using the scripting environment of ABAQUS software, with random coding generated in Python to ensure a realistic and random distribution of fibers. Figure 5 shows an example of generated curved recycled fibers, namely, concrete with fibers with a random distribution. The RSFs are randomly distributed in the specimen volume, and this dispersion is such that none of the fibers interfere with each other.

Interaction definition between the RSFs and CNT-modified UHPC

To simulate the damage and separation phenomena between microfibers and composites, the cohesive zone model (CZM) theory was employed. The CZM model relies on load−displacement curves to model damage and separation phenomena in this area. This approach allows for the representation of the mechanical behavior of interfaces between microfibers and the composite matrix, capturing the initiation and propagation of damage under loading conditions. By utilizing CZM, researchers can analyze the evolution of damage, predict failure modes, and assess the mechanical performance of composite materials with microfibers. This modeling technique provides valuable insights into the behavior of fiber-reinforced composites and aids in the design and optimization of such materials for various engineering applications. Using the traction–separation law constructed by the bilinear CZM, the mechanical performance of the bonding apparent is simulated. In the absence of any failure, as shown in Fig. 6, the contact surface is assumed to behave linearly. The linear behavior disappears with the occurrence of failure. In the model, three parameters can consider all the mechanisms of the bonding process: a) the maximum shear stress or strength of the bonding area (σ_{max}), b) the maximum critical separation strain (δ_{in}), and (c) *the* exponential parameter n in the fracture zone. By calibrating the results of the MSFEM with the experimental test results, these three parameters are determined.

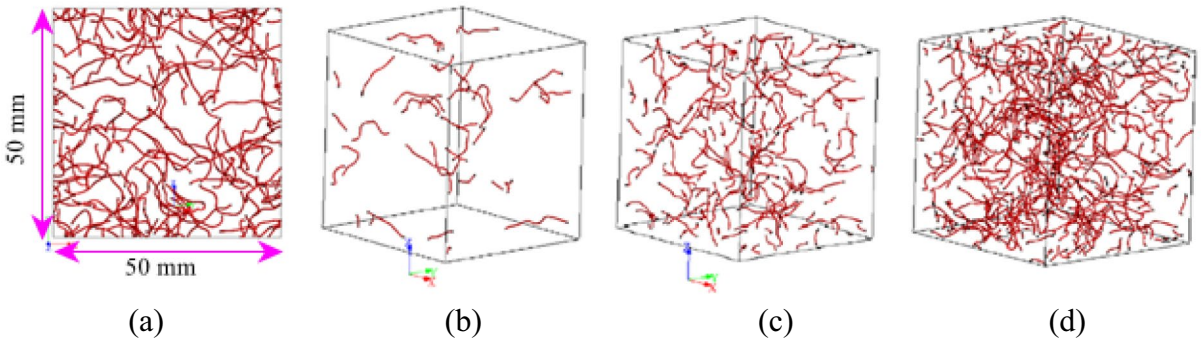

Figure 5. (**a**) 2D view of simulated RSFs in the form of curved cylinders with different lengths and RSF geometries with random distributions for (**b**) 0.2 wt.%, (**c**) 0.4 wt.%, and (**d**) 0.8 wt.%

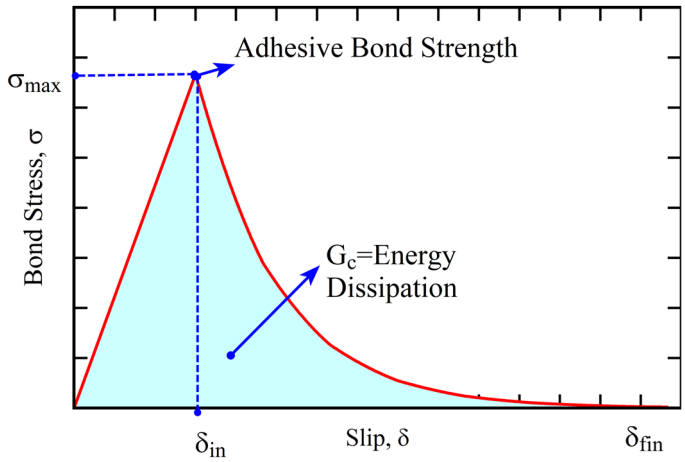

Figure 6. The bond stress with slip changes in the adhesion zone.

Mechanical properties of the materials

To simulate the mechanical performance of CNT-modified UHPC, a concrete damaged plasticity (CDP) model was applied. For four UHPC specimens with different cement weight fractions, the mechanical properties were determined by performing uniaxial compressive tests and direct tensile tests, which are shown in Figs. 7 and 8 as stress–strain diagrams and tensile curves for specimens with 0, 0.2, 0.4 and 0.8 wt.% carbon nanotubes. RSFs and steel bars behave in an elastic–plastic manner, and their characteristics are taken into account in the modeling process according to Table 4 and Fig. 3. In ABAQUS software, the CDP model can be defined using fundamental parameters including the ratio of biaxial strength f_{bo} to uniaxial strength f_{co} in compression, the failure surface parameter K, dilation angle ψ, eccentricity ε, and viscosity μ. Table 4 presents these parameters for the CDP model used in the simulation.

Load protocol, boundary conditions and meshing

In the present study, to expand the experimental test results, finite element modeling of the ribbed steel bar pull-out test was implemented. The pull-out test for the steel bar is simulated in 3D using ABAQUS software. To consider more realistic expectations in 3D models, bonding elements are used to define the chemical adhesion between the ribbed bar and concrete. To validate the numerical models, the initial finite element outcomes are compared with the experimental test results, and the finite element models are calibrated. In this research, for the first time, the rib of a steel bar is simulated, and in Fig. 9, an MSFEM of a specimen with boundary and loading conditions is shown. In the studied models, according to the experimental model, the top surface of the concrete specimens is completely bound, and a displacement of up to a maximum of 20 mm is applied to the upper part of the steel bar. The specimen was stretched under a loading speed of 0.2 mm/min. Because the areas around the steel bars are more sensitive, finer elements have been used in these areas. In finite element models, 10-node nonlinear three-dimensional solid elements (C3D10M) are utilized for meshing, and the nonlinear quasistatic method is used to analyze the model. Static, General with nonlinear geometry consideration, a time

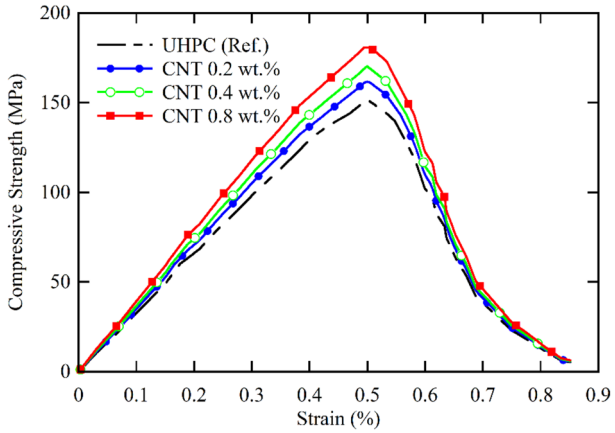

Figure 7. Compressive strength–strain curves of four UHPC specimens with 0, 0.2, 0.4 and 0.8 wt.% CNTs.

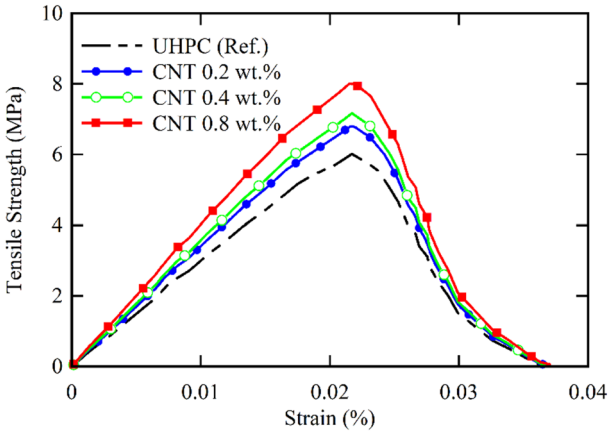

Figure 8. Direct tensile stress–strain curves for four UHPC specimens with 0, 0.2, 0.4 and 0.8 wt.% CNTs.

CNT content (wt.%)	E (GPa)	ν	ψ	ε	fb0/fc0	K	μ
0.0	48.8	0.20	32	0.1	1.11	0.667	0.001
0.2	49.9	0.22	35	0.1	1.10	0.667	0.001
0.4	50.8	0.22	38	0.1	1.07	0.667	0.001
0.8	52.2	0.24	41	0.1	1.06	0.667	0.001

Table 4. Values used for the non-linear parameters in CDP model for UHPC reinforced with CNTs.

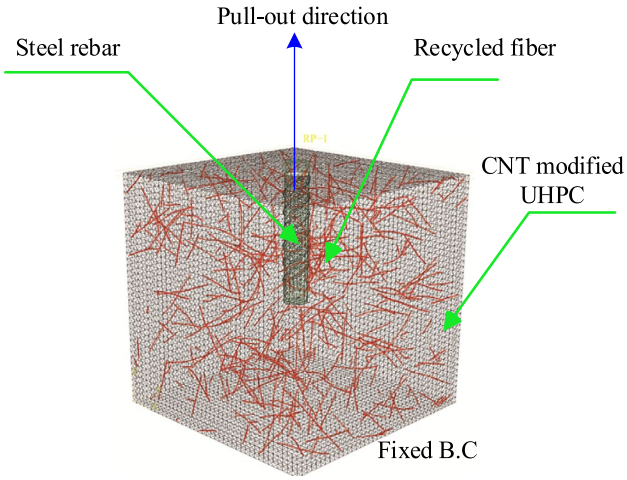

Figure 9. Multiscale pull-out finite element model with boundary and loading conditions.

period of 1.0 s, an initial increment size of 0.01 s, and minimum and maximum increment sizes of 1e-5 s and 0.01 s, respectively, were chosen to ensure accurate and stable simulations. Convergence in this context refers to the ability of the iterative algorithm, typically the Newton–Raphson method, to achieve equilibrium between external and internal forces at the end of a load increment, within a predefined numerical tolerance. Due to the simulation of the rebar ribs, the mesh size of the RSFs, cohesion layer and concrete close to the ribs should be small enough to accurately represent the deformation and stress gradients. The appropriate dimensions of the elements are determined after checking the mesh independence.

Results and discussion

CZM parameters and MSFEM validation

Using experimental tests, the parameters for the CZM are calculated. In the next step, the impact of several factors on the pull-out performance and bond strength of ribbed steel bars with CNT-modified UHPC is investigated. Interaction constraints and descriptions of adhesive elements were used to determine the interactions

between the fibers and the concrete. The CZM parameters are clarified since the load–displacement graph came by the MSFEM is consistent with the outcomes of pull-out experiments on a 14 mm diameter steel bar from CNT-modified UHPC. Following the calibration of the results, the mechanical properties of the CZM were determined, as presented in Table 5. Figure 10 presents the load–slip curve of the final finite element model and the experimental outcomes of specimens with 0 and 1% volume fractions of fibers based on the values provided in Table 5. The experimental test outcomes and MSFEM outcomes overlap favorably both in terms of the shape of the curve and the maximum pull-out load, with a difference of less than 4% in the maximum pull-out load among the experimental results and MSFEM results. Therefore, the MSFEM accurately predicts the pull-out performance of ribbed steel bars from UHPC and can be used to investigate the influence of some parameters.

Pull-out failure mechanism

An investigation of the load–slip curve (Fig. 10) shows that for the same characteristics of the steel bar, using fibers significantly enhances the bonding between the steel bar and the concrete. Accordingly, for steel bars with a diameter of 14 mm, the maximum bond strengths of high-strength concrete at 0% and 1% of the fiber volume fraction are 52.5 kN and 73.6 kN, respectively, indicating that the use of 1% of the fiber volume fraction increases the bond strength of concrete by 40.15%, which can be regarded as an increase in the mechanical load

	σ_{max}	δ_{in}	G_c
Steel fiber	7.45 MPa	1.4×10^{-3} mm	0.67 MPa mm
Rebar steel	153 MPa	2.3×10^{-3} mm	1.84 MPa mm

Table 5. CZM values of the RSFs and ribbed steel bars with CNT-modified UHPC.

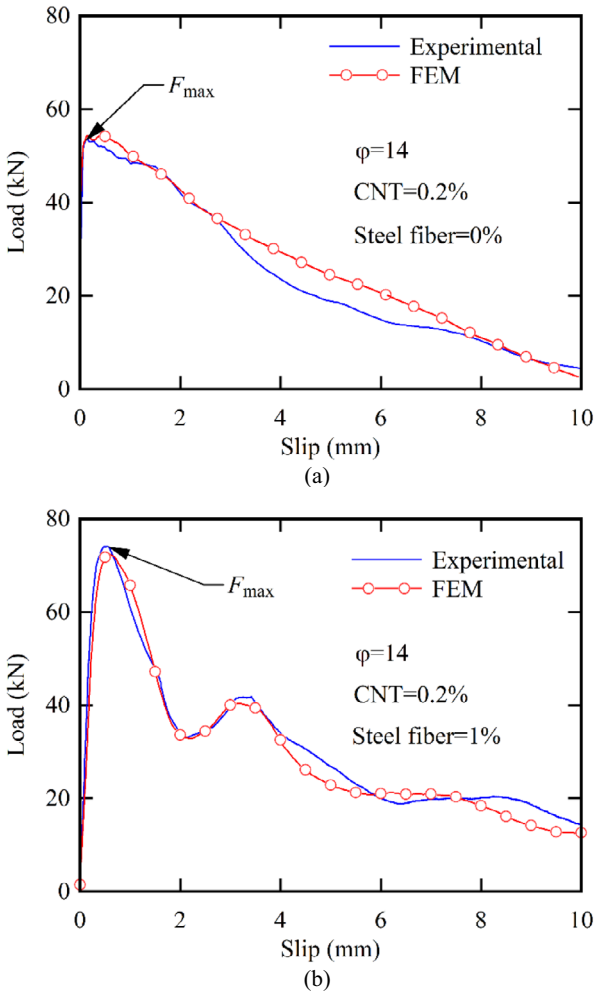

Figure 10. Experimental and finite element load-slip curves of the ribbed bar pull-out test of fiber-reinforced UHPC with 0.2% CNT, (**a**) 0% fiber content and (**b**) 1% fiber content.

as a result of adding fibers to the concrete. According to literature[22,27,28], the load-slip curve of the ribbed steel bar has three components: friction stability, chemical adhesion, and interlocking action with shear bonding. At the beginning of the test, the primary mechanism of resistance to external loads is chemical adhesion among the bar and concrete, and at this stage, no-slip motion can be measured. The chemical bond between the concrete and the ribbed bar joints weakens with increasing load, and factors such as frictional stability and mechanical bonding among the concrete and joints increase the bond strength. Then, due to the shear bonding of the steel bar, it maintains its connection with the concrete. Among the joining mechanisms, the mechanical bonding of the ribbed bar to the concrete is of significance since it presents the most significant bond stress. The load is transmitted through the steel bar ribbed and concrete jags between them in this coupling mechanism. Therefore, compression stress occurs where the steel bar ribs meet the concrete treads, resulting in tensile ring stresses in the cross-section of the concrete around the steel bar and shear stresses in the concrete gaps among the treads. According to this stress field, there are two types of coupling failure modes. The steel bar will be pulled out of the concrete if the shear stress between the concrete joints and the steel bar ribbed exceeds the final shear strength of the concrete. Suppose that the tensile strength of the tensile ring exceeds the tensile strength of the concrete before the concrete jags are crushed between the two consecutive ribbeds of the steel bars. In that case, radial cracks will form in the concrete around the steel bar, eventually causing the concrete cover around the steel bar to be shredded and the concrete specimen to break. At this stage of the bonding behavior of the concrete and ribbed steel bars, the effect of friction on the capacity of the final bonding load is negligible, resulting in brittle and sudden failure. This type of connection failure is called splitting. Figure 11 shows two different types of failures in the fiber-reinforced concrete specimens with a 1% fiber volume fraction.

Figure 12 shows the stress distribution in three separate phases of fiber, ribbed steel bar, and concrete for the UHPC specimen with 1% fiber by volume fraction at a load of 60 kN. As seen, in the presence of fibers and the bridging action between fibers and concrete, the applied load to the concrete is also distributed in the fibers. As a result, considerable stresses are created in the fibers. The fibers absorb a significant portion of the transfer load to the concrete and thus meaningfully increase the mechanical characteristics of the concrete and its bonding behavior with the steel bar. According to the stress distribution in the ribbed steel bar presented in Fig. 12, due to the more remarkable mechanical restraint of the steel bar with concrete, the maximum stress created in the steel bar is in the place of the treads.

Figure 13 illustrates the distribution of failure and the process of pulling out a ribbed steel bar from UHPC containing a 1% volume fraction of fibers. The three distinct areas highlighted in the figure are friction bonding, mechanical bonding, and maximum pull-out load. At the onset of the applied tensile load, all regions of the concrete in contact with the steel bar experience stress. This stress distribution reflects the initial stages of the pull-out process, where the concrete undergoes deformation and damage as the steel bar is subjected to tensile forces. The friction bonding region represents the interface between the steel bar and the UHPC matrix, where adhesion between the materials is prominent. The mechanical bonding region depicts the area where mechanical interlocking between the steel bar and UHPC occurs, contributing to enhanced bond strength. Finally, the maximum pull-out load region indicates the point at which the applied load reaches its peak value, signifying the maximum resistance offered by the concrete-steel interface before failure occurs. Overall, Fig. 13 provides valuable insights into the behavior of UHPC and the interaction between steel bars and the UHPC matrix during the pull-out process. By overcoming chemical and frictional bonding loads, the breakdown distribution in concrete gradually increases. As the applied load increases, the chemical bonding loads disappear entirely. The rebar begins to separate from the concrete, in which case the mechanical restraint formed in the position of the rebar edges creates local points of load transfer among the fibers and the matrix. As a result, due to the greater strength of the rebar, its treads cause the destruction of the concrete in the areas around the rebar, as shown in Fig. 13c. Based on the pull-out performance of the ribbed steel rebar from UHPFRC, it has been observed that slip occurs outward depending on the frictional strength of the fibers. As a result, in this case, the failure will be of the sliding type shown in Fig. 13d. In addition to frictional stability and chemical bonding, mechanical

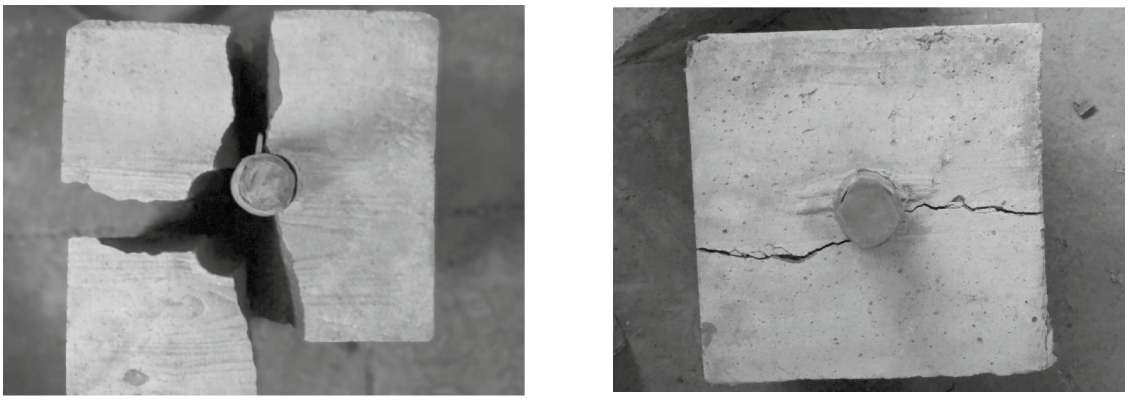

Figure 11. (**a**) Splitting pattern of the UHPC sample without RSFs (**b**) Splitting failure of UHPC sample with 1% of RSFs.

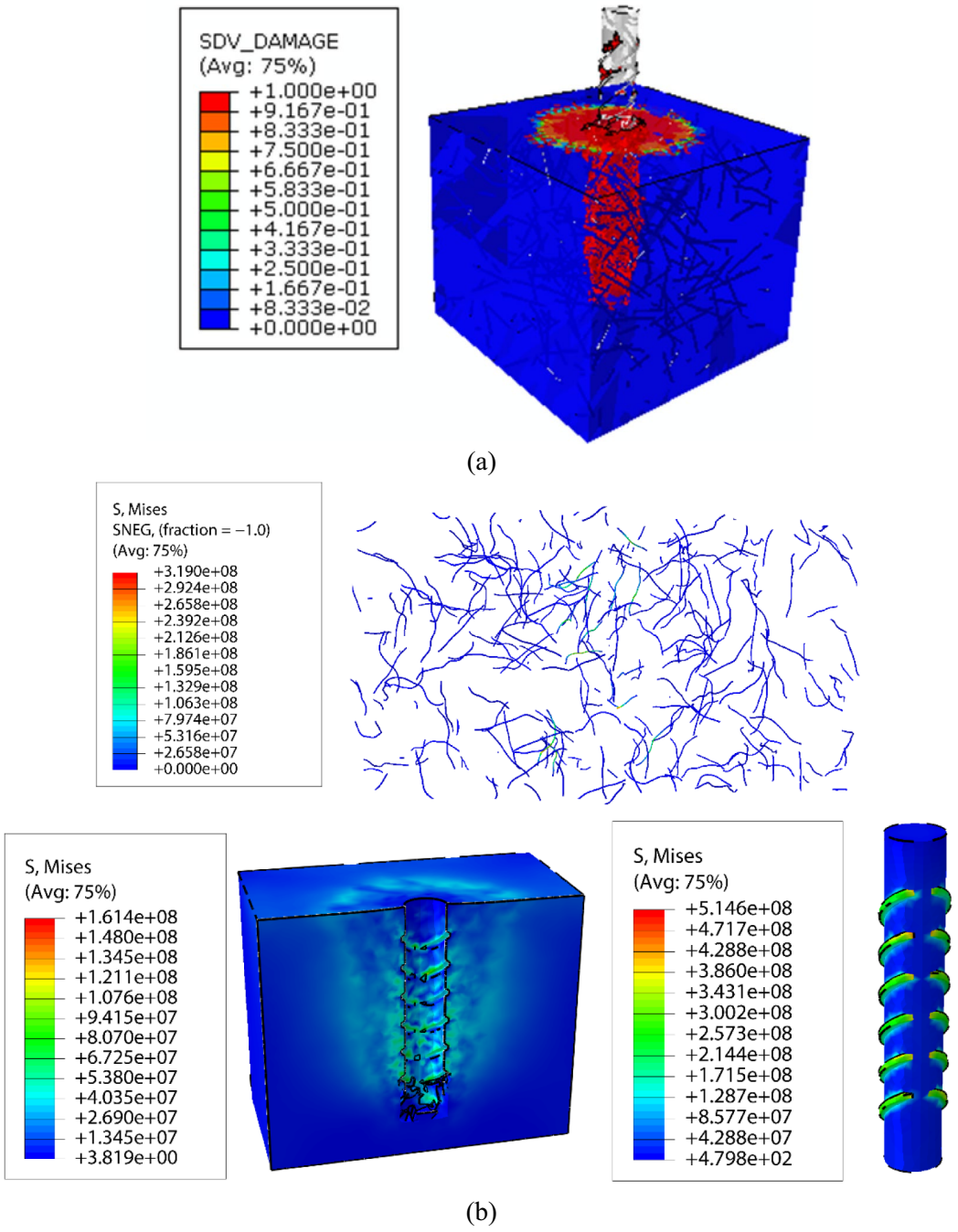

Figure 12. (**a**) Breakdown distribution in three separate phases of RSFs, steel rebar, and UHPC specimen with 1 wt.% RSFs and at the load of 60 kN, (**b**) Stress (Pa) distributions in different three phase.

bonding between the concrete and tread part of the rebar increases the bond strength of the ribbed bars. The shear coupling of steel bars with concrete is noteworthy among the coupling mechanisms since it generates the maximum coupling stress. In this bonding mechanism, load transfer is terminated by engaging the tread section and concrete jags among them.

Pull-out response

In this section, for a more detailed study of the impact of bond length and rebar diameter, the bonding behavior of rebar and UHPFRC is studied. Figures 14 and 15 show the impact of the nanoparticle weight fraction of the cement and the volume fraction of the RSFs on the load—slip curves. The results show that these two parameters significantly affect the bond performance of rebar, and with increasing amounts of carbon nanotubes and RSFs, the pull-out load similarly increases. According to the outcomes of Fig. 14, for a volume fraction of RSFs equal to 0.5% and 2%, the maximum pull-out loads are 62.8 kN and 97.4 kN, respectively, which indicates an increase

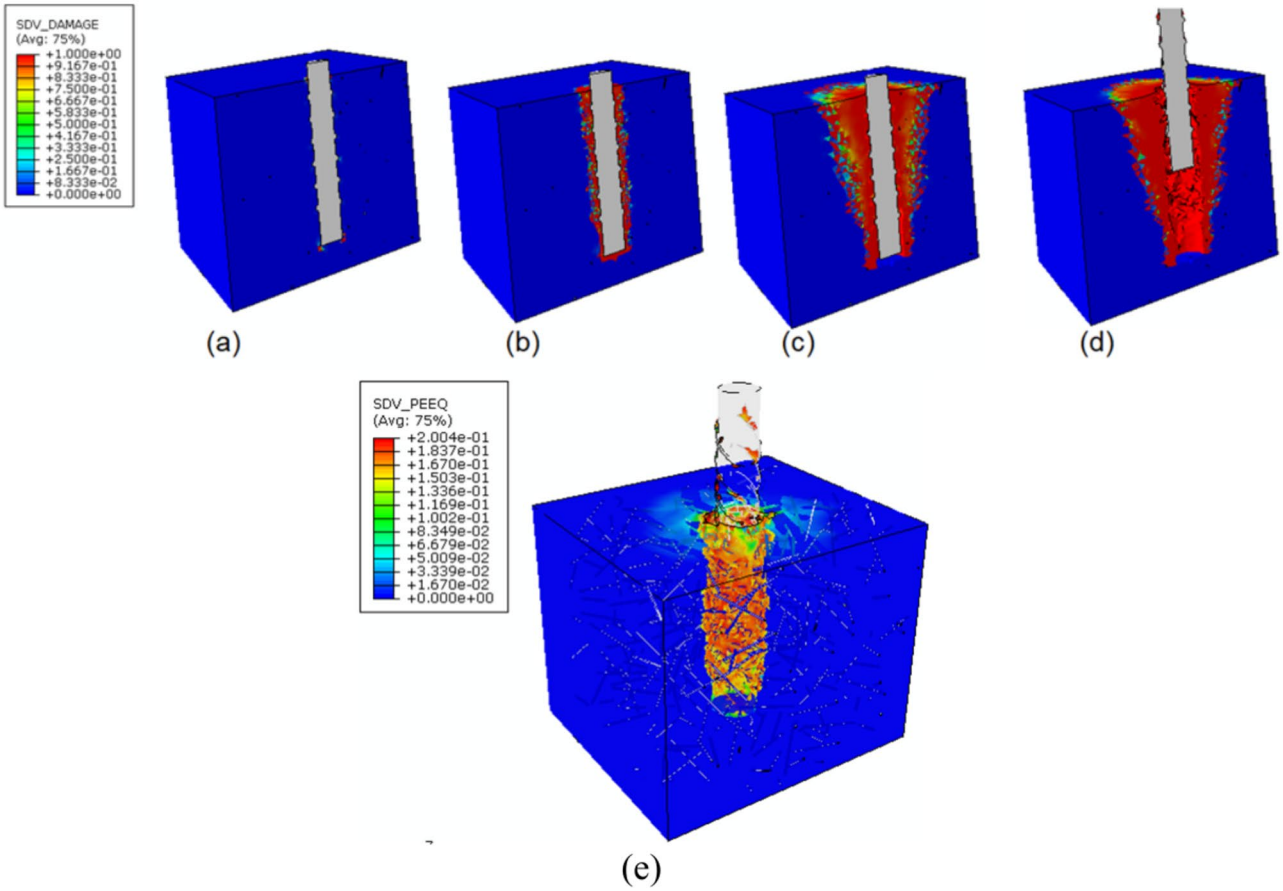

Figure 13. Damage distribution in the three zones: (**a**) the friction bonding, (**b**) the mechanical bonding, (**c**) maximum pull-out load, and (**d**) final behavior after pull-out, and (**e**) defective strain distribution in concrete and recycled steel fibers.

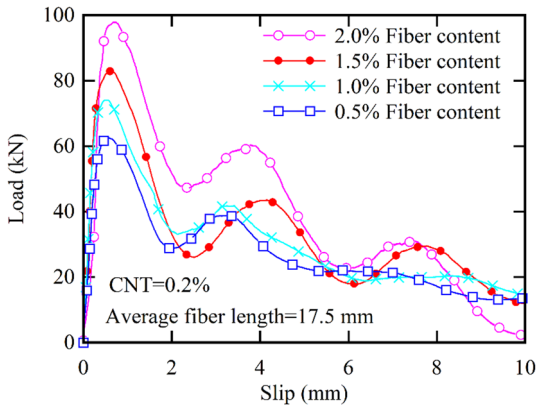

Figure 14. Impact of the volume fraction of recycled steel fibers on the load-slip curves of steel bars and UHPC.

of approximately 55% in the pull-out load. Similar results can be seen regarding the influence of CNTs on the bond strength, according to Fig. 15. Increasing the amount of carbon nanotubes increases the load required to cause bond failure. Given that increasing the amount of carbon nanotubes by bridging prevents the growth of microcracks, it is reasonable to improve the final bond strength. For 1% recycled steel fibers, when the amount of carbon nanotubes increases from 0% to 0.8%, the final bond strength increases from 70.2 kN to 108.8 kN, which indicates an increase of approximately 55% in the pullout load. The results of the study indicate that when

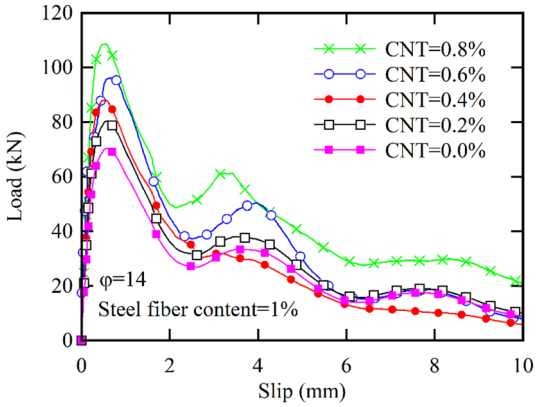

Figure 15. Influence of the CNT volume fraction on the load—slip curves of the steel bar and UHPC specimens.

the maximum coupling stress is reached, the load-bearing mechanism is lost, and the remaining joint strength depends mainly on the frictional resistance.

Another interesting result observed in Figs. 14 and 15 is the presence of secondary peaks in the pullout force–displacement curves. These peaks are attributed to the treads on the rebar, which cause mechanical interlocking and interaction between the rebar and UHPFRC. As the fiber content increases, the force at these positions also rises, due to the role of recycled steel fibers in enhancing the concrete's resistance to crack growth and failure. For instance, for concrete with 0.5% and 2% fibers, the secondary peak force is 38.5 and 60.1 kN, respectively, indicating a 56% increase. A similar trend is evident regarding the effect of CNTs, as shown in Fig. 15. With the increase in nanoparticle weight fraction from 0 to 0.8%, the secondary peak force rises from 33.6 to 61.8 kN, representing an 84% improvement due to the presence of carbon nanotubes.

After performing finite element analysis and investigating the failure of the specimens, it was found that according to Fig. 16, the steel bars slipped out of the high-strength fiber concrete, and none of the steel bars reached the yield stress. Additionally, according to Fig. 16, as the amount of fibers used in the concrete mix increases, the maximum stress created in the rebar also increases, and this maximum stress is created around the rebar.

Another parameter that affects the bonding of steel bars and UHPC is the aspect ratio of the fibers, as shown in Fig. 17, which affects the load-slip curve. The outcomes show that by increasing the aspect ratio of the fibers, the impact of adding fibers on improving the final bonding load decreases. For example, as the aspect ratio of the fibers increased from 87.5 to 120, the final bond strength increased by approximately 12%. By decreasing the RSF aspect ratio from 87.5 to 60, the final bond strength increases by approximately 6.8%. With decreasing aspect ratio, the number of fibers used increases, so for a constant volume fraction, fibers with a low aspect ratio prevent the growth of microcracks in UHPC and thus improve the bond strength of steel bars to UHPC. In contrast, fibers with higher aspect ratios are more effective against the development of macrocracks and prevent the complete failure of concrete.

Table 6 provides a more detailed analysis of the impacts of several factors on the bond characteristics of steel bars with UHPFRC. The volume fraction of fibers, aspect ratio, and weight fraction of carbon nanotubes affect the pull-out variables, including the pull-out load slip linked with the maximum load point, pull-out energy absorption, and effective pull-out bond stress. Increasing the volume fraction of fibers and weight fraction of CNTs increases the pull-out load and pull-out work. This result is the opposite of that for the aspect ratio.

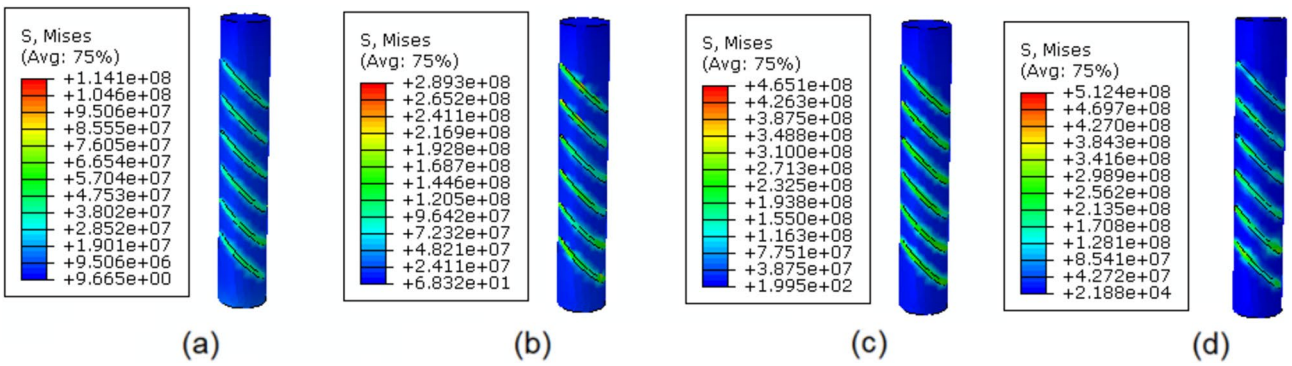

Figure 16. Stress distribution in steel bars located in UHPFRC containing 1% recycled steel fibers and (**a**) 0 wt.% carbon nanotubes, (**b**) 0.2% CNT, (**c**) 0.6% CNT and (**d**) 0.8% CNT.

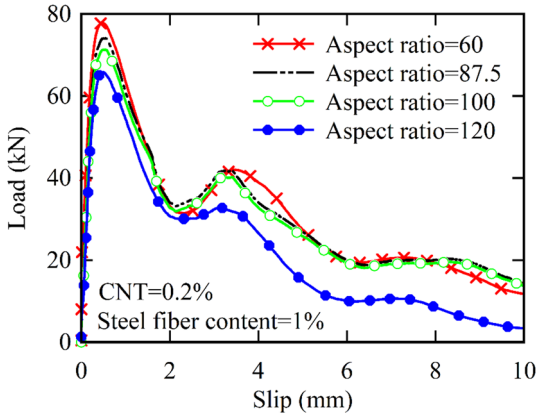

Figure 17. Load–slip curves of specimens containing steel microfibers with different aspect ratios.

Fiber content (%)	CNT content (%)	Fiber aspect ratio	Pull-out load (kN)	Critical separation (mm)	Pullout work (kN/mm)	Bond stress (MPa)
0	0.2	87.5	48.3	0.311	281	313.92
0.5			62.6	0.542	282	406.86
1.0			74.3	0.503	317	482.91
1.5			82.8	0.605	346	538.15
2.0			97.8	0.701	398	635.64
1	0	87.5	70.3	0.578	273	456.91
	0.2		74.3	0.503	317	482.91
	0.4		88.3	0.512	285	573.90
	0.6		96.9	0.703	382	629.79
	0.8		108.3	0.509	506	703.89
1	0.2	60	78.6	0.475	324	510.85
		87.5	74.3	0.503	317	482.91
		100	70.6	0.510	301	458.86
		120	66.4	0.486	221	431.56

Table 6. Effect of the aspect ratio of the recycled steel fibers, the amount of fibers and the amount of carbon nanotubes on the pullout load, critical separation, pullout energy absorption, and effective pullout bond stress.

Additionally, for 1% of the fibers, as the amount of carbon nanotubes increased from 0 to 0.8%, the pull-out bond stress and pull-out work increased by approximately 85% and 103%, respectively. In addition, it was observed that the bonding stress decreases with increasing fiber aspect ratio. However, the opposite is true for the volume fraction of fibers, and as the amount of fibers used in UHPFRC increases, the bonding stress increases. Thus, the use of steel fibers with a lower aspect ratio (steel microfibers) significantly improves the pull-out characteristics of ribbed steel bars from concrete. The results indicate that both recycled steel fibers and carbon nanotubes significantly enhance the pullout force in UHPFRC, which corresponds to improved resistance to cracking and failure. The presence of these materials strengthens the mechanical bond between the rebar and concrete, leading to higher secondary peak forces in the pullout force–displacement curves. This improvement can be attributed to the enhanced mechanical interlocking provided by the treads on the rebar and the reinforcing effects of the added fibers and nanoparticles.

Conclusion

In the present study, the pull-out behavior of ribbed steel bars from CNT-modified UHPFRC was studied using MSFEM. The interaction between fibers and concrete and between steel bars and concrete is simulated using the CZM concept, whose factors are derived from the experimental outcomes of steel bar pull-out tests. Additionally, in the MSFEM, the structure consists of three separate phases: 1) CNT-modified UHPC that is considered uniform, and its mechanical properties are extracted from experimental test outcomes of direct tensile tests and compressive strength tests and introduced to the software. 2) Recycled steel fibers in the form of curved cylinders of constant diameter and different lengths are randomly distributed within the volume fraction of the concrete body. 3) The area of the interface between the fibers and the concrete and between the rebar and the concrete is simulated using the CZM model. After validating the FEMs with experimental data, the impacts of the fiber

aspect ratio, fiber volume fraction, and carbon nanotube weight fraction on the adhesion characteristics of ribbed steel bars with UHPFRC were investigated. The key outcomes of the present study are as follows:

- For volume fractions of recycled steel fibers equal to 0.5% and 2%, the maximum pull-out loads are 62.8 kN and 97.4 kN, respectively, which indicates an increase of approximately 55% in the pull-out load.
- Increasing the carbon nanotube weight fraction increases the load required to cause bond failure. As the amount of carbon nanotubes increases, the weight fraction increases from 0% to 0.8%, and the final bond strength increases by approximately 55%.
- By increasing the aspect ratio of the fibers, the effect of adding the fibers on improving the final bonding load decreases. For example, as the aspect ratio of the fibers increased from 87.5 to 120, the final bond strength increased by approximately 12%. By decreasing the fiber aspect ratio from 87.5 to 60, the final bond strength increases by approximately 6.8%.
- By reducing the aspect ratio, the number of fibers used increases, so for a constant volume fraction, fibers with a lower aspect ratio prevent the growth of microcracks in concrete and thus improve the bond strength of steel bars to concrete. In contrast, fibers with a larger aspect ratio are more effective against the growth of macrocracks and prevent the complete failure of concrete.

Since the experimental test results show an error of less than 4% in the maximum pull-out load compared to that of the specimen finite element model, the MSFEM accurately predicts the pullout performance of steel bars from UHPC. By utilizing this method, it is possible to investigate the effect of many effective parameters without having to perform costly and time-consuming experimental tests.

Data availability

Data sets generated during the current study are available from the corresponding author on reasonable request.

Received: 29 April 2024; Accepted: 25 July 2024
Published online: 27 August 2024

References

1. Almustafa, M. K. & Nehdi, M. L. Machine learning prediction of structural response of steel fiber-reinforced concrete beams subjected to far-field blast loading. *Cement Concr. Compos.* **126**, 104378 (2022).
2. Zhang, J., Wu, Z., Yu, H., Ma, H. & Da, B. Mesoscopic modeling approach and application for steel fiber reinforced concrete under dynamic loading: A review. *Engineering* **16**, 220–238 (2022).
3. Li, L. *et al.* Experimental and numerical investigation on impact dynamic performance of steel fiber reinforced concrete beams at elevated temperatures. *J. Build. Eng.* **47**, 103841 (2022).
4. Aghaee, K. & Khayat, K. H. Effect of shrinkage-mitigating materials on performance of fiber-reinforced concrete—An overview. *Constr. Build. Mater.* **305**, 124586 (2021).
5. Amran, M. *et al.* Fiber-reinforced alkali-activated concrete: A review. *J. Build. Eng.* **45**, 103638 (2022).
6. Lakshmi, A., Pandit, P., Bhagwat, Y. & Nayak, G. A review on efficiency of polypropylene fiber-reinforced concrete. *Sustain. Trends Chall. Civ. Eng. Sel. Proc. CTCS* **2020**, 799–812 (2022).
7. Morampudi, P., Namala, K. K., Gajjela, Y. K., Barath, M. & Prudhvi, G. Review on glass fiber reinforced polymer composites. *Mater. Today Proc.* **43**, 314–319 (2021).
8. Ramakrishnan, T., Babu, M. S., Balasubramani, S., Manickaraj, K. & Jeyakumar, R. Effect of fiber orientation and mechanical properties of natural fiber reinforced polymer composites—A review. *Paideuma J.* **14**(3), 17–23 (2021).
9. Nguyen, T.-T., Thai, H.-T. & Ngo, T. Optimised mix design and elastic modulus prediction of ultra-high strength concrete. *Constr. Build. Mater.* **302**, 124150 (2021).
10. Banthia, N., Majdzadeh, F., Wu, J. & Bindiganavile, V. Fiber synergy in hybrid fiber reinforced concrete (HyFRC) in flexure and direct shear. *Cem. Concr. Compos.* **48**, 91–97 (2014).
11. Sabbaghian, M. & Kheyroddin, A. Experimental Investigation of the effect of fiber on mechanical properties and the age of high-performance fiber reinforced cement composites. *Concr. Res.* **12**(4), 53–68 (2019).
12. Ghone, M. O., Long, G., Yang, K., Ma, X. & Islam, N. Toughness improvement of low strength ceramsite lightweight concrete by polypropylene fiber and recycled rubber particle. *Constr. Build. Mater.* **422**, 135716 (2024).
13. Isa, M., Pilakoutas, K., Guadagnini, M. & Angelakopoulos, H. Mechanical performance of affordable and eco-efficient ultra-high performance concrete (UHPC) containing recycled tyre steel fibres. *Constr. Build. Mater.* **255**, 119272 (2020).
14. Aram Partan, M., Eskandari, H., Lezgy-Nazargah, M. & Gharouni Nik, M. Evaluating the effect of forta and polypropylene fibers on compressive strength, ductility and energy absorption of cylindrical concrete specimens. *Concr. Res.* **14**(2), 53–67 (2021).
15. Huang, H. *et al.* Effect of carbon nanotube and graphite nanoplatelet on composition, structure, and nano-mechanical properties of CSH in UHPC. *Cem. Concr. Res.* **154**, 106713 (2022).
16. Zhou, Z. & Qiao, P. Bond behavior of epoxy-coated rebar in ultra-high performance concrete. *Constr. Build. Mater.* **182**, 406–417 (2018).
17. Khaksefidi, S., Ghalehnovi, M. & De Brito, J. Bond behaviour of high-strength steel rebars in normal (NSC) and ultra-high performance concrete (UHPC). *J. Build. Eng.* **33**, 101592 (2021).
18. Khosravi, S. & Goudarzi, M. A. Seismic risk assessment of on-ground concrete cylindrical water tanks. *Innov. Infrastruct. Solut.* **8**(1), 68 (2023).
19. Khosravi, S., Yousefi, M. M. & Goudarzi, M. Development of seismic fragility curves of cylindrical concrete tanks using nonlinear analysis. *Amirkabir J. Civ. Eng.* **53**(1), 71–88 (2021).
20. Karimzadeh, F., Ziaei-Rad, S. & Adibi, S. Modeling considerations and material properties evaluation in analysis of carbon nanotubes composite. *Metall. Mater. Trans. B* **38**, 695–705 (2007).
21. Ayatollahi, M., Shadlou, S. & Shokrieh, M. Multiscale modeling for mechanical properties of carbon nanotube reinforced nanocomposites subjected to different types of loading. *Compos. Struct.* **93**(9), 2250–2259 (2011).
22. Esmaeili, J., Andalibi, K., Gencel, O., Maleki, F. K. & Maleki, V. A. Pull-out and bond-slip performance of steel fibers with various ends shapes embedded in polymer-modified concrete. *Constr. Build. Mater.* **271**, 121531 (2021).
23. Bouhala, L., Makradi, A., Belouettar, S., Younes, A. & Natarajan, S. An XFEM/CZM based inverse method for identification of composite failure parameters. *Comput. Struct.* **153**, 91–97 (2015).

24. Rilem, T. RC 6 Bond test for reinforcement steel. 2. Pull-out test, 1983. RILEM recommendations for the testing and use of constructions materials, 218–220 (1994).
25. Carvalho, E. P., Ferreira, E. G., Cunha, J. C. D., Rodrigues, C. D. S. & Maia, N. D. S. Experimental investigation of steel-concrete bond for thin reinforcing bars. *Latin Am. J. Solids Struct.* **14**(11), 1932–1951 (2017).
26. Xiao, J. *et al.* Probabilistic models applied to concrete corrosion depth prediction under sulfuric acid environment. *Measurement* **234**, 114807 (2024).
27. Jin, Q., Wang, G., Liang, T. & Chen, P. Bond-slip behavior between GFRP bars and mortar based on pull-out tests. *Polym. Composites* **40**(7), 2840–2849 (2019).
28. Xu, L., Wang, X., Pan, J., Zhou, J. & Liu, W. Bond behavior between steel-FRP composite bars and engineered cementitious composites in pullout conditions. *Eng. Struct.* **299**, 117086 (2024).

Author contributions
All authors contributed in software, analysis, data gathering, writing, and conception. Amir Ebrahim Akbari Baghal provided critical revisions, statistical analysis, experimental setup and approved the final version of the paper.

Competing interests
The authors declare no competing interests.

Additional information
Correspondence and requests for materials should be addressed to F.K. or V.A.M.

Reprints and permissions information is available at www.nature.com/reprints.

Publisher's note Springer Nature remains neutral with regard to jurisdictional claims in published maps and institutional affiliations.